General polarizability and hyperpolarizability estimators for the path-integral Monte Carlo method applied to small atoms, ions, and molecules at finite temperatures

Juha Tiihonen, Ilkka Kylänpää, and Tapio T. Rantala
Department of Physics, Tampere University of Technology, P.O. Box 692, FI-33101 Tampere, Finland
(Received 27 July 2016; published 26 September 2016)

The nonlinear optical properties of matter have a broad relevance and many methods have been invented to compute them from first principles. However, the effects of electronic correlation, finite temperature, and breakdown of the Born-Oppenheimer approximation have turned out to be challenging and tedious to model. Here we propose a straightforward approach and derive general field-free polarizability and hyperpolarizability estimators for the path-integral Monte Carlo method. The estimators are applied to small atoms, ions, and molecules with one or two electrons. With the adiabatic, i.e., Born-Oppenheimer, approximation we obtain accurate tensorial ground state polarizabilities, while the nonadiabatic simulation adds in considerable rovibrational effects and thermal coupling. In both cases, the 0 K, or ground-state, limit is in excellent agreement with the literature. Furthermore, we report here the internal dipole moment of PsH molecule, the temperature dependence of the polarizabilities of H^-, and the average dipole polarizabilities and the ground-state hyperpolarizabilities of HeH^+ and $H_3{}^+$.

DOI: 10.1103/PhysRevA.94.032515

I. INTRODUCTION

Obtaining nonlinear optical properties (NOP) of matter by computational simulation is particularly important in such environments that are out of reach with experimental studies. For instance, this applies to exotic light-nucleus molecules like $H_3{}^+$ and HeH^+ in hot and dense stars and gas planets [1–3], or short lifetime particles like Ps or PsH [4–6]. Quite a different but trending regime is that of computational biophysics, where the accurate effects of polarization, finite temperature, and dielectric solvents are required of the molecular interaction models [7]. Motivations for the computational study of the NOP are diverse, and they are properly summarized in dedicated reviews [8–11].

The first-principles treatment of dielectric response comes down to dipole and multipole moments and polarizabilities. Basically, the computation of tensorial polarizabilities is straightforward, and a lot of methods have been developed for this purpose over the years, e.g., Refs. [12–23]. The significance of polarizabilities is pronounced in many physical scales starting from microscopic interactions, such as van der Waals [24], to macroscopic properties, like dielectric constant and refractive index. Transformation from the molecular to the optical level is typically an emergent procedure that loses some of the tensorial detail to statistical averaging of properties. The density of the effective polarizable medium is then related to the bulk with Clausius-Mossotti or Lorentz-Lorenz relations. Thus, in principle, one could build up macroscopic NOP in specific conditions simply by computing and combining the right set of microscopic polarizabilities. In practice, this can get tedious.

For example, consider a diatomic homonuclear molecule, like H_2, that has two distinct dipole polarizabilities α_{zz} and α_{xx}. Combined, they make up a rotationally averaged, effective polarizability $\bar{\alpha}$ that is well suited for the macroscopic transformation. However, anisotropy of the electronic polarizability is strongly coupled with the rovibrational state of the system, and to address this, the breakdown of the Born-Oppenheimer approximation is needed. The conventional way is to form the total polarizability out of the electronic, rotational, and vibrational parts [8], the latter of which are unique for every rovibrational state. When it comes to modeling the thermal coupling of properties, the relevant ensemble of excited states is required. This has lead to systematic tabulation of rovibrational state contributions, e.g., Ref. [25], which is surely informative but becomes quickly overwhelming with higher temperatures and more complicated systems. Thus, for simulating the NOP in thermal conditions, the most reasonable course of action is to reduce complexity. This can be done by making approximations or using semiempirical methods, e.g., Refs. [26,27]. The more controllable way is to give up the tensorial character and concentrate directly on the average properties [28] or the exact thermal ensemble.

In this paper, we provide a tangible interface between tensorial distinction and thermal averaging of molecular polarizabilities. We perform a series of path-integral Monte Carlo (PIMC) simulations on a variety of small atoms and molecules: H, Ps, He, H^-, Li^+, PsH, $H_2{}^+$, H_2, $H_3{}^+$, and HeH^+. Similar study for H and H_2 was done earlier with finite field approach [29], but this time we propose field-free static polarizability and hyperpolarizability estimators for imaginary-time path-integral methods. The exact account of particle correlations in PIMC is a useful feature for two reasons: electronic correlation is important to the accurate evaluation of polarizabilities [30], and nuclear correlation allows a controlled breakdown of the Born-Oppenheimer approximation. Also, inherent account of thermal ensemble allows direct sampling in finite temperature and, in principle, at finite density. That being said, PIMC is probably the most straightforward way to simulate thermal coupling of polarizabilities from first principles.

II. THEORY

Consider a quantum statistical system with N distinguishable particles in phase space R. The state of the system is described by finite-temperature density matrix ρ. The density operator is

$$\hat{\rho} = e^{-\hat{H}/k_B T}, \tag{1}$$

where $\hat{H}$ is the Hamiltonian operator. In the path-integral picture, we identify $\hbar/k_B T = \beta = i(t - t_0)$ as an imaginary-time interval, so that we can write Eq. (1) in terms of action $\hat{S} = \beta\hat{H}$. Any diagonal observable $\langle O\rangle$ can be obtained by integrating the relevant operator $\hat{O}$ over the phase space

$$\langle O\rangle = Z^{-1}\int dR\langle R|\hat{\rho}|R\rangle O(R), \tag{2}$$

where

$$Z = \int dR\langle R|\hat{\rho}|R\rangle \tag{3}$$

is the partition function.

Now, consider a perturbation caused by a uniform external electric field F_α, where indices $\alpha,\beta,\gamma,\delta,\ldots$, follow the Einstein summation over the axes x, y, and z. In uniform field, the perturbation of the Hamiltonian is completely described by

$$\hat{H}^{(1)} = \hat{H}^{(0)} - \hat{\mu}_\alpha F_\alpha, \tag{4}$$

where $\hat{H}^{(0)}$ is the unperturbed Hamiltonian and $\hat{\mu}_\alpha$ is the dipole moment operator. According to the Buckingham convention [31], the change in total energy is written as a perturbation expansion of coefficients

$$E^{(1)} = E^{(0)} + \mu_\alpha F_\alpha + \tfrac{1}{2}\alpha_{\alpha\beta}F_{\alpha\beta} + \tfrac{1}{6}\beta_{\alpha\beta\gamma}F_{\alpha\beta\gamma} + \tfrac{1}{120}\gamma_{\alpha\beta\gamma\delta}F_{\alpha\beta\gamma\delta} + \cdots. \tag{5}$$

Hence, in the zero-field limit, we can solve the individual properties:

$$\mu_\alpha = \lim_{F\to 0}\frac{\partial}{\partial F_\alpha}E^{(1)}, \tag{6}$$

$$\alpha_{\alpha\beta} = \lim_{F\to 0}\frac{\partial}{\partial F_\alpha}\frac{\partial}{\partial F_\beta}E^{(1)} = \lim_{F\to 0}\frac{\partial}{\partial F_\beta}\mu_\alpha, \tag{7}$$

$$\beta_{\alpha\beta\gamma} = \lim_{F\to 0}\frac{\partial}{\partial F_\alpha}\frac{\partial}{\partial F_\beta}\frac{\partial}{\partial F_\gamma}E^{(1)} = \lim_{F\to 0}\frac{\partial}{\partial F_\gamma}\alpha_{\alpha\beta}, \tag{8}$$

$$\gamma_{\alpha\beta\gamma\delta} = \lim_{F\to 0}\frac{\partial}{\partial F_\alpha}\frac{\partial}{\partial F_\beta}\frac{\partial}{\partial F_\gamma}\frac{\partial}{\partial F_\delta}E^{(1)} = \lim_{F\to 0}\frac{\partial}{\partial F_\delta}\beta_{\alpha\beta\gamma}, \tag{9}$$

and so on. Bearing in mind that $\frac{\partial\hat{S}}{\partial F_\alpha} = \beta\hat{\mu}_\alpha$, direct differentiation eventually leads to the following exact tensorial estimators:

$$\alpha_{\alpha\beta} = \beta[\langle\mu_\alpha\mu_\beta\rangle - \langle\mu_\alpha\rangle\langle\mu_\beta\rangle], \tag{10}$$

$$\beta_{\alpha\beta\gamma} = \beta^2\left[\langle\mu_\alpha\mu_\beta\mu_\gamma\rangle + 2\langle\mu_\alpha\rangle\langle\mu_\beta\rangle\langle\mu_\gamma\rangle - \sum_{\alpha\beta,\gamma}\langle\mu_\alpha\mu_\beta\rangle\langle\mu_\gamma\rangle\right], \tag{11}$$

$$\gamma_{\alpha\beta\gamma\delta} = \beta^3\left[\langle\mu_\alpha\mu_\beta\mu_\gamma\mu_\delta\rangle - 6\langle\mu_\alpha\rangle\langle\mu_\beta\rangle\langle\mu_\gamma\rangle\langle\mu_\delta\rangle - \sum_{\alpha\beta\gamma,\delta}\langle\mu_\alpha\mu_\beta\mu_\gamma\rangle\langle\mu_\delta\rangle - \sum_{\alpha\beta,\gamma\delta}\langle\mu_\alpha\mu_\beta\rangle\langle\mu_\gamma\mu_\delta\rangle + 2\sum_{\alpha\beta,\gamma,\delta}\langle\mu_\alpha\mu_\beta\rangle\langle\mu_\gamma\rangle\langle\mu_\delta\rangle\right], \tag{12}$$

where shorthand notation is used for unique terms with cyclic permutation over comma-separated indices, e.g.,

$$\sum_{\alpha\beta,\gamma}\langle\mu_\alpha\mu_\beta\rangle\langle\mu_\gamma\rangle = \langle\mu_\alpha\mu_\beta\rangle\langle\mu_\gamma\rangle + \langle\mu_\gamma\mu_\alpha\rangle\langle\mu_\beta\rangle + \langle\mu_\beta\mu_\gamma\rangle\langle\mu_\alpha\rangle.$$

It should be pointed out that the bracketed terms on the right-hand side, e.g., $\langle u_\alpha\rangle$, are the relevant observables for a path-integral simulation. That is, in this form the polarizability estimates, e.g., $\langle\alpha_{\alpha\beta}\rangle$, cannot be computed directly from a single sample trajectory. Rather, they emerge from the correct addition of the long-time expectation values of different dipole moment products.

III. METHOD

In path-integral Monte Carlo scheme, integration of phase space is carried out by Monte Carlo sampling of discrete imaginary-time paths. The path of length β is discretized according to the expansion [32], which divides the length into small intervals: $\beta = M\tau$, where M is the Trotter number. Calculation of diagonal properties can then be done by taking average of each time slice:

$$\langle O\rangle = M^{-1}Z^{-1}\sum_{i=1}^{M}\langle R_{i-1}|\rho(R_{i-1},R_i;\tau)|R_i\rangle O(R_i), \tag{13}$$

where R_i are the coordinates of particles at the ith time slice, and $R_0 = R_M$. This is exact in the limit of $\tau\to 0$, or $M\to\infty$, but for practical reasons finite time step is used. The best accuracy is obtained by using the so-called pair approximation to describe Coulomb interaction [33]. Correct and efficient sampling of the density operator $\rho(R_{i-1},R_i;\tau)$ near the thermal equilibrium is obtained by Metropolis Monte Carlo with multilevel bisection procedure [34]. In this paper, only systems with up to two electrons are considered. Thus opposite spins are assumed, and all the particles obey Boltzmann statistics [5].

The total energies are obtained by thermal or virial estimators [35]. The virial estimator is preferred, because it has smaller variance. However, for convenience the thermal estimator is used for adiabatic simulations with more than one fixed nucleus. The polarizabilities are computed according to the dipole moment products that appear in Eqs. (10)–(12). The dipole moment is unambiguously defined for the neutral systems, where the effect of the origin cancels out. For the systems with a nonzero net charge, we set the origin at the

center-of-mass of the nuclei, or that of all the particles, in adiabatic or nonadiabatic simulations, respectively.

IV. RESULTS

We investigate a few well-known small atoms, ions, and molecules with up to two electrons by performing parallel PIMC simulations. By fixing or freeing the nuclear motion we demonstrate the breakdown of the Born-Oppenheimer approximation. The inclusion of the electron-nuclei coupling reveals the rovibrational effects, and thus, together with finite temperature, also the thermal coupling of properties. This allows us to report the total energies and relevant tensorial polarizabilities corresponding to both the electronic ground state and the finite-temperature rovibrational ensemble. Due to the exponential nature of thermal effects, we approach the observed thermal trends with an *ad hoc* exponential least-squares fit of the form

$$O = a\ \exp(bT) + c, \tag{14}$$

where O is the observable and a, b, and c are the fitting parameters.

In any case, the number of nonvanishing and distinguishable tensor properties is greatly reduced by symmetry. To best convey with the literature, we use z to mark the principal direction, and, when suitable, x for a perpendicular direction. None of the studied systems require more than two simultaneous directions. Capital Z is used to denote the laboratory axis, which is used in freely rotating nonadiabatic simulations. Statistical standard error of the mean (SEM) with 2σ, i.e., 2SEM confidence boundaries are used unless otherwise stated.

When relevant, we use $m_p = 1836.15267248 m_e$ for proton mass and $m_{\mathrm{He}} = 7294.2995363 m_e$ for that of He nucleus. Generally, the time step of $\tau = 0.03$ is sufficient for the systems with only hydrogen, and any small discrepancy with the literature is due to the high temperature. For heavier nuclei, i.e., He and Li^+, also smaller time step of $\tau = 0.01$ is used, but it accounts for a small error in total energy. In some simulations, especially the nonadiabatic, $\tau = 0.1$ is used for computational feasibility, but also to demonstrate the time-step effect, or lack thereof.

A. Adiabatic simulations

The adiabatic, i.e., fixed-nuclei calculations, are good to begin with, since they exhibit no thermal coupling by default: the most stable systems, i.e., the neutral and the positive, are effectively at their electronic ground states at thousands of kelvins [48]. High temperature is preferred for computational feasibility, and thus 2000 K is used for the simulation of H, Ps, He, H_2, Li^+, H_2^+, H_3^+, and HeH^+. PsH is less stable because of the highly mobile positron and is simulated at 1000 K. The most special case is the hydrogen negative ion, whose polarizabilities show notable temperature dependency at relatively low temperatures; H^- is simulated at 25–500 K and the results are extrapolated to 0 K.

For each adiabatic simulation we report the time step, the total energy, and all the relevant polarizability tensors depending on the symmetry. Also, the best available 0 K references from the literature are shown for comparison [29,36–47,49–59]. The simplest group is presented in Table I; atoms and ions with a single fixed nucleus are isotropic and have no permanent dipole moment, and thus they only have nonvanishing dipole polarizability α_{zz} and second hyperpolarizability γ_{zzzz}. The total energies match at least with three, and most of the polarizabilities at least with two significant digits. The biggest discrepancies are with the extrapolated values of H^-, which could stem from the choice of the extrapolation function (14). The temperature dependencies of α_{zz} and γ_{zzzz} of H^- are presented in Fig. 1, and it is likely that instead of exponential decay, α_{zz} would saturate towards the reference value. Also, to our knowledge, γ_{zzzz} has been reported for neither of the positron systems, Ps and PsH, prior to this work.

TABLE I. Time steps τ, total energies E, and static dipole polarizabilities α_{zz} and second hyperpolarizabilities γ_{zzzz} obtained from the adiabatic calculations of atoms and ions are matched with suitable literature references.

	τ	E	α_{zz}	γ_{zzzz}
Ps	0.03	−0.24999(2)[a]	36.00(4)[a]	1.70(4) × 10^5[a]
		−0.25[b]	36[b]	1.7067 × 10^5[b]
H	0.03	−0.49996(2)[a]	4.502(4)[a]	1331(28)[a]
	0.03	−0.49997(5)[c]	4.496(23)[c]	1586(184)[c]
		−0.5[d]	4.5[d]	1333.1[e]
H^-	0.1	−0.52799(6)[f]	206(2)[f]	7.4(2.9) × 10^7[f]
	0.03	−0.52781(7)[f]	209(5)[f]	5.9(7.0) × 10^7[f]
		−0.52775[g]	206.15[h]	8.03 × 10^7[i]
PsH	0.03	−0.78932(7)[a]	42.27(7)[a]	1.60(8) × 10^5[a]
		−0.78913[j]	42.2836[k]	
He	0.01	−2.9036(2)[a]	1.382(4)[a]	42(6)[a]
		−2.90372[l]	1.38319217[m]	43.104[m]
Li^+	0.01	−7.2810(4)[a]	0.1923(4)[a]	0.24(8)[a]
		−7.279913[n]	0.192453[n]	0.2427[p]

[a]This work.
[b]E, α_{zz}, and γ_{zzzz} of Ps are half, 8-fold, and 128-fold of those of H, respectively.
[c]Tiihonen *et al.* [29].
[d]Waller [36].
[e]Sewell [37].
[f]This work (extrapolated to 0 K).
[g]Lin [38]; Nakashima *et al.* [39].
[h]Kar *et al.* [40].
[i]Pipin *et al.* [41].
[j]Frolov *et al.* [42].
[k]Yan [43].
[l]Pekeris [44]; Nakashima *et al.* [39].
[m]Cencek *et al.* [45].
[n]Johnson *et al.* [46].
[p]Grasso *et al.* [47].

Table II contains homonuclear molecules and molecular ions made of protons and electrons. They also lack the permanent dipole moment, but now the geometry gives rise to optical anisotropy, i.e., difference between the response in z and x directions. Consequently, the nonvanishing terms are $\alpha_{zz} \neq \alpha_{xx}$ and $\gamma_{zzzz} \neq \gamma_{xxxx} \neq \gamma_{zzxx} \neq \gamma_{xxyy}$ [31]. The simulations of the diatomic molecules were carried out at the approximate equilibrium bond lengths $R_{H_2^+} = 2.0 a_0$ and $R_{H_2} = 1.4 a_0$ so that the nuclei were connected by the z axis.

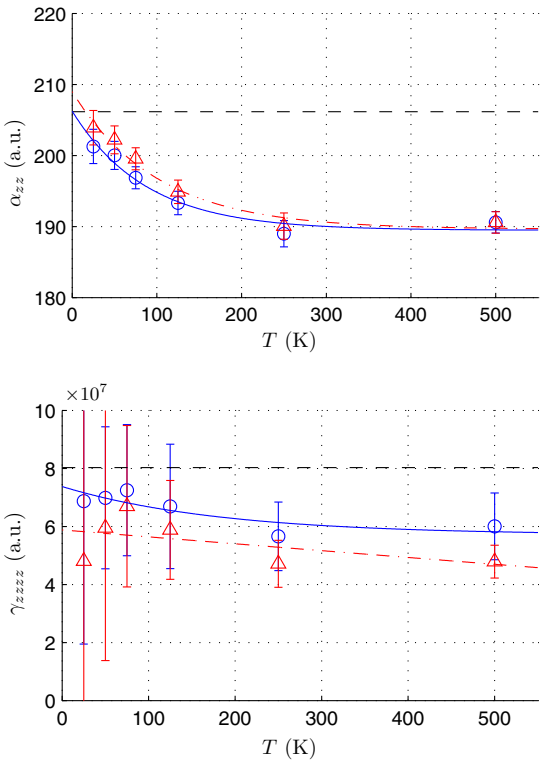

FIG. 1. Finite temperature data for α_{zz} and γ_{zzzz} of H^- is plotted against temperature for two time steps: $\tau = 0.1$ (blue circle) and $\tau = 0.03$ (red triangle). Exponential fit is used to extrapolate to 0 K. The black dashed lines mark reference values at 0 K [40,41].

The nuclei in triangular H_3^+ molecule were fixed equilaterally $R_{H_3^+} = 1.65a_0$ apart so that the z axis was perpendicular to the plane. Again, the agreement of the total energy is good. With H_2^+ and H_2, the agreement is also good with the polarizabilities. The latest and the only references of the dipole polarizability of H_3^+ are from Ref. [57], where they are assumed inaccurate lower-bound estimates. Indeed, our results for α_{zz} and α_{xx} are somewhat larger. We also present estimates for the higher static polarizabilities of H_3^+.

The most complicated of our systems is HeH^+, because it contains a permanent dipole moment μ_z, which also induces nonzero first hyperpolarizabilities $\beta_{zzz} \neq \beta_{zxx}$. With nonzero net charge, the choice of origin for the dipole moment is ambiguous. Here, we use the center-of-mass of the nuclei, which places the origin $0.293609a_0$ apart from the He nucleus with the equilibrium bond length of $R_{HeH^+} = 1.46a_0$. All of the properties are presented in Table III, and up to the dipole polarizabilities they match well with the literature. None of the hyperpolarizabilities have been reported before, although the error boundaries are very dominant with any of the z-dependent components.

Vaguely in the spirit of Ref. [60], we also performed a simulation of PsH as sort of a molecule consisting of two electrons and two "nuclei," proton and positron. By replacing the laboratory axis with the local axis between the nuclei, we were able to compute a nonzero dipole moment of $\mu_z = 0.0305(6)$. In principle, such treatment of PsH causes slight alterations to the properties of PsH found in Table I and a symmetry similar to that of HeH^+. To demonstrate such small effects, more laborious calculations would be required, but we omit the opportunity for now. The essence of this work is to show that the proposed estimators give decent values for polarizabilities and hyperpolarizabilities, and so far this requirement has been amply met.

B. Nonadiabatic simulations

An important step towards realistic and more meaningful simulation of nonlinear optical properties is the breakdown of the Born-Oppenheimer approximation. In PIMC, this is done by allowing quantum statistical description of the nuclei, i.e., replacing fixed-point charges with imaginary-time trajectories similar to the electrons. Besides reduced mass correction to electron-nucleus interaction, this enables the exact account

TABLE II. Time step τ, total energies E, and static anisotropic dipole polarizabilities $\alpha_{zz} \neq \alpha_{xx}$ and second hyperpolarizabilities $\gamma_{zzzz} \neq \gamma_{xxxx} \neq \gamma_{zzxx} \neq \gamma_{xxyy}$ obtained from the adiabatic calculations of homonuclear molecules and molecular ions are matched with suitable literature references.

	τ	R	E	α_{zz}	α_{xx}	γ_{zzzz}	γ_{xxxx}	γ_{zzxx}	γ_{xxyy}
H_2^+	0.03	2.0	−0.60259(10)[a]	5.080(4)[a]	1.7586(8)[a]	−43(17)[a]	73(2)[a]	27(2)[a]	24.2(5)[a]
			−0.602634214[b]	5.0776490[c]	1.757648[c]	−193.76[d]	83.87[d]	29.73[d]	
H_2	0.03	1.4	−1.1746(4)[a]	6.388(7)[a]	4.574(5)[a]	700(49)[a]	572(26)[a]	211(10)[a]	191(7)[a]
	0.03		−1.17434(18)[e]	6.382(13)[e]	4.577(10)[e]	787(100)[e]	640(73)[e]		
			−1.17447477[f]	6.387493[g]	4.57861[g]	682.5[g]	575.9[g]	211.9[g]	192.0[g]
H_3^+	0.03	1.65	−1.3438(3)[a]	2.202(2)[a]	3.549(3)[a]	51(4)[a]	58(11)[a]	19(2)[a]	19(3)[a]
			−1.3438356[h]	1.7322[i]	3.2923[i]				

[a]This work.
[b]Turbiner *et al.* [49]; Laaksonen *et al.* [50]; Madsen *et al.* [51].
[c]Tsogbayar *et al.* [52].
[d]Bishop *et al.* [53].
[e]Tiihonen *et al.* [29].
[f]Kolos *et al.* [54].
[g]Bishop *et al.* [55].
[h]Turbiner *et al.* [56].
[i]Kawaoka [57].

TABLE III. Permanent dipole moment and static dipole polarizabilities and hyperpolarizabilities from the adiabatic simulation of HeH^+ molecular ion with $\tau = 0.01$.

E	μ_z	α_{zz}	α_{xx}	β_{zzz}	β_{zxx}	γ_{zzzz}	γ_{xxxx}	γ_{zzxx}	γ_{xxyy}
−2.9785(6)[a]	0.6788(1)[a]	1.544(21)[a]	0.8515(7)[a]	−2(4)[a]	−0.17(7)[a]	11(507)[a]	7.2(8)[a]	3(8)[a]	2.4(2)[a]
−2.978706[b]	0.655[b]	1.5421[c]	0.85070[c]						

[a]This work.
[b]Pachucki [58].
[c]Pavanello *et al.* [59].

of rovibrational motion in thermal bath. On the downside, we are not able to distinguish between rotational, vibrational, and electronic components directly, unless we use artificial constraints and internal coordinates. Yet, here we aim at skipping the tedious tabulation and explicit summation of rovibrational properties and, instead, get the accurate and thermally averaged estimates served on a silver platter.

We simulated four isolated molecules, namely H_2^+, H_2, H_3^+ and HeH^+, in various temperatures. The maximum temperature was 1600 K (3200 K for H_2), where molecular stability is still sustained; dissociation of molecules would result in an undesired explosion in the variance of the dipole moment products. In Table IV we summarize the obtained total energies and make polynomial extrapolations to 0 K. Comparison with the literature [28,58,61–65] shows that the agreement in total energies is good at least with the smaller time step $\tau = 0.03$, although the results of HeH^+ might be improved by a smaller time step still. The average bond lengths are altered by the rovibrational motion. Extrapolation to 0 K gives $R_{H_2^+} = 2.0630(9)a_0$, $R_{H_2} = 1.4482(4)a_0$, $R_{H_3^+} = 1.7231(6)a_0$, and $R_{HeH^+} = 1.5167(4)a_0$ with $\tau = 0.03$.

In laboratory coordinates with freely moving nuclei, all the odd terms, i.e., μ and β, vanish due to symmetry and the anisotropic properties, i.e., α and γ, reduce to orientational averages. In Fig. 2, we present the temperature dependencies of the average dipole polarizability α_{ZZ} and second hyperpolarizability γ_{ZZZZ} for each molecule. The data points are accompanied with a least-squares nonlinear fit according to Eq. (14). Extrapolated values, i.e., $\alpha_{ZZ}(0) = a + c$, are presented in Table V and compared with the literature, when possible. It appears that all of the homonuclear systems exhibit similar behavior: α_{ZZ} increases by the temperature in linear or quadratic fashion, and the effect is to some extent countered with exponential decay of γ_{ZZZZ}. The explanation is simple, if we assume that the primary contribution to γ_{ZZZZ} is given by the rotational states. The rotational hyperpolarizability emerges from the anisotropy between α_{zz} and α_{xx}: the molecule has a tendency to assume more favorable orientation, which is that of higher α. Typically, the lowest rotational states have the highest hyperpolarizabilities [25], and thus the dominant part γ_{ZZZZ} is decreased as the thermal ensemble shifts towards higher temperatures. Out of the homonuclear systems, H_2^+ goes through the most drastic change in γ_{ZZZZ}, and it has indeed the highest anisotropy.

HeH^+ has different response to the temperature: α_{ZZ} decays by the temperature and γ_{ZZZZ} seems to tend to zero as the temperature is increased. This is surely influenced by the permanent dipole moment μ_z. Even though μ_Z and β_{ZZZ}

TABLE IV. Total energies from nonadiabatic calculations of molecules with two time steps $\tau = 0.1$ and $\tau = 0.03$. The values are extrapolated to 0 K and compared values from the literature.

	τ	0 K	200 K	400 K	800 K	1600 K	3200 K
H_2^+	0.1	−0.5972(8)[a]	−0.59668(6)[b]	−0.59599(6)[b]	−0.59445(9)[b]	−0.59007(9)[b]	
	0.03	−0.5975(12)[a]	−0.59682(9)[b]	−0.59599(9)[b]	−0.59438(12)[b]	−0.59006(15)[b]	
		−0.597139[c]					
H_2	0.1	−1.16518(12)[a]	−1.16456(9)[b]	−1.16394(10)[b]	−1.16256(8)[b]	−1.15952(16)[b]	−1.15050(13)[b]
	0.03	−1.16436(16)[a]	−1.16374(15)[b]	−1.16300(12)[b]	−1.16163(12)[b]	−1.15850(19)[b]	−1.14340(21)[b]
		−1.164025[d]					
H_3^+	0.1	−1.3245(2)[a]	−1.3239(2)[b]	−1.3228(2)[b]	−1.3207(2)[b]	−1.3133(3)[b]	
	0.03	−1.3233(3)[a]	−1.3226(3)[b]	−1.3217(3)[b]	−1.3192(3)[b]	−1.3118(3)[b]	
		−1.323568[e]					
HeH^+	0.1	−2.9827(3)[a]	−2.9823(3)[b]	−2.9815(2)[b]	−2.9803(2)[b]	−2.9761(3)[b]	
	0.03	−2.9722(5)[a]	−2.9717(4)[b]	−2.9712(4)[b]	−2.9697(4)[b]	−2.9656(5)[b]	
		−2.96627[f]					

[a]This work (extrapolated to 0 K).
[b]This work.
[c]Tang *et al.* [28].
[d]Stanke *et al.* [61].
[e]Kylänpää *et al.* [62] ([63]).
[f]Calculated based on Refs. [58] and [64].

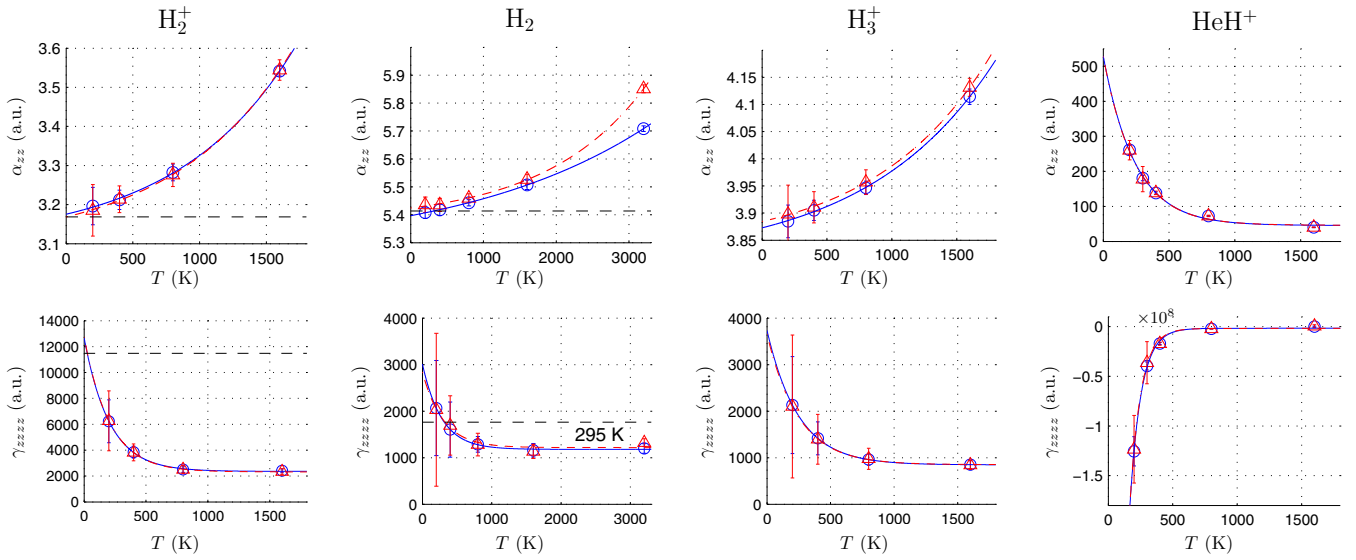

FIG. 2. Nonadiabatic dipole polarizabilities α_{ZZ} and second hyperpolarizabilities γ_{ZZZZ} are plotted against the temperature. Blue circles and red triangles mark the simulated data points associated with $\tau = 0.1$ and $\tau = 0.03$, respectively. Least-squares nonlinear fits have been made according to Eq. (14). When available, the black dashed lines mark reference values at 0 K [28,65] or 295 K [25].

vanish in the nonadiabatic ensemble, the existence of μ_z induces large rotational component for α_{ZZ}, likewise to the previous paragraph. Thus, when the anisotropy of μ gets decreased by higher-order rotational motion, so does the rotational part of α_{ZZ}.

At this point it is fair to note, however, that any qualitative ideas concerning the rotational or vibrational components are inspired by previous works, and no such conclusions can be drawn solely from the raw simulation data of this work. What is evident, though, is that the difference between the adiabatic and the nonadiabatic results is huge. This is not an implication of error but of the importance of nonadiabatic effects and thermal coupling.

V. SUMMARY

We have derived general estimators of static dipole polarizabilities and hyperpolarizabilities for the path-integral Monte Carlo method. Using the field-free estimators is straightforward in any kind of molecular simulation, and it surpasses our previous finite-field approach in simplicity and speed [29]. In principle, the computation of nonlinear optical properties of matter can be done with PIMC directly at any finite temperature.

As a reference, a variety of well-known one- and two-electron atoms and molecules were simulated with PIMC: H, Ps, H^-, He, Li^+, H_2^+, H_2, PsH, H_3^+, and HeH^+. Agreement with the literature is mostly excellent, with the exceptions of H^- and H_3^+, whose static dipole polarizabilities are being improved in this work. Also, we provide tensorial estimates of the second hyperpolarizabilities of PsH, H_3^+, and HeH^+ and hyperpolarizabilities of HeH^+. While our list of two-electron systems is not exhaustive, the efficiency and universality of our method is still amply demonstrated.

Beyond the computation of adiabatic, or fixed-nuclei polarizabilities, we take two important steps with unprecedented ease: the breakdown of the Born-Oppenheimer approximation brings in dielectric contributions emerging from nuclear motion, and the sampling of thermal ensemble couples them directly to finite temperature. We estimate the temperature dependencies of the polarizabilities of four molecules: H_2^+, H_2, H_3^+, and HeH^+ between 0 and 1600 kelvin (3200 K for H_2). Again, we demonstrate good agreement with the literature, if one exists. The explicit treatment of thermal averaging gives rise to interesting relationships between the anisotropic and the average quantities, e.g., anisotropy $\alpha_{zz} \neq \alpha_{xx}$ induces large rotational component to γ_{ZZZZ}, which then decays rapidly by the temperature.

Clearly, PIMC is a special method that allows exact simulation of polarizabilities in novel regimes. The accuracy of results is controllable by computational effort, whose limitations are evident but not really imminent in the scope of our work. Partly for this reason but mainly for the

TABLE V. Polarizabilities and hyperpolarizabilities from nonadiabatic calculations of atoms are extrapolated to 0 K by using Eq. (14).

	τ	α_{ZZ}	γ_{ZZZZ}
H_2^+	0.1	3.175(34)[a]	12674(1006)[a]
	0.03	3.168(49)[a]	12750(1403)[a]
	ref.	3.168725[b]	11479.805[b]
H_2	0.1	5.397(19)[a]	3012(604)[a]
	0.03	5.424(24)[a]	2839(894)[a]
	ref.	5.4139[c]	
H_3^+	0.1	3.873(24)[a]	3738(642)[a]
	0.03	3.884(39)[a]	3656(950)[a]
HeH^+	0.1	529(8)[a]	$-1.128(8)\times10^9$[a]
	0.03	528(23)[a]	$-1.202(21)\times10^9$[a]

[a]This work (extrapolated to 0 K).
[b]Tang *et al.* [28].
[c]Kolos *et al.* [65].

simplicity, the higher multipole properties and the effects of finite density and pressure were left out of this work. Same goes for solids and more complicated molecules, such as H_2O or CO_2, even though the power of PIMC resides in the accurate many-body correlations. This work is best reviewed as a necessary first step on the path of understanding the quantum statistical dielectric properties with PIMC.

ACKNOWLEDGMENTS

We thank David Ceperley for insightful discussions. For financial support we gratefully acknowledge the Jenny and Antti Wihuri Foundation, and the Academy of Finland. Also, we acknowledge CSC–IT Center for Science Ltd. and Tampere Center for Scientific Computing for the allocation of computational resources.

[1] G. J. Harris, A. E. Lynas-Gray, S. Miller, and J. Tennyson, Astrophys. J. **600**, 1025 (2004).
[2] G. J. Harris, A. E. Lynas-Gray, S. Miller, and J. Tennyson, Astrophys. J. **617**, L143 (2004).
[3] E. A. Engel, N. Doss, G. J. Harris, and J. Tennyson, Mon. Not. R. Astron. Soc. **357**, 471 (2005).
[4] D. B. Cassidy and A. P. Mills, Nature (London) **449**, 195 (2007).
[5] I. Kylänpää, T. T. Rantala, and D. M. Ceperley, Phys. Rev. A **86**, 052506 (2012).
[6] A. P. Mills, J. Phys.: Conf. Ser. **488**, 012001 (2014).
[7] I. V. Leontyev and A. A. Stuchebrukhov, J. Chem. Theory Comput. **8**, 3207 (2012).
[8] D. M. Bishop, Rev. Mod. Phys. **62**, 343 (1990).
[9] D. P. Shelton and J. E. Rice, Chem. Rev. **94**, 3 (1994).
[10] G. Maroulis, *Atoms, Molecules, and Clusters in Electric Fields: Theoretical Approaches to the Calculation of Electric Polarizability* (Imperial College Press, London, 2006).
[11] J. Mitroy, M. S. Safronova, and C. W. Clark, J. Phys. B **43**, 202001 (2010).
[12] A. Dalgarno and J. T. Lewis, Proc. R. Soc. A **233**, 70 (1955).
[13] D. W. Norcross and M. J. Seaton, J. Phys. B: At. Mol. Phys. **9**, 2983 (1976).
[14] A. Hibbert, M. L. Dourneuf, and V. K. Lan, J. Phys. B: At. Mol. Phys. **10**, 1015 (1977).
[15] R. McWeeny, Int. J. Quantum Chem. **23**, 405 (1983).
[16] B. Kirtman, J. M. Luis, and D. M. Bishop, J. Chem. Phys. **108**, 10008 (1998).
[17] K. Pachucki and J. Sapirstein, Phys. Rev. A **63**, 012504 (2000).
[18] C. C. Cannon and A. Derevianko, Phys. Rev. A **69**, 030502 (2004).
[19] X. Chu and A. Dalgarno, J. Chem. Phys. **121**, 4083 (2004).
[20] M. Safronova and W. Johnson, Adv. At., Mol., Opt. Phys. **55**, 191 (2008).
[21] L.-Y. Tang, Z.-C. Yan, T.-Y. Shi, and J. F. Babb, Phys. Rev. A **79**, 062712 (2009).
[22] A. L. Hickey and C. N. Rowley, J. Phys. Chem. A **118**, 3678 (2014).
[23] J. Kobus, Phys. Rev. A **91**, 022501 (2015).
[24] J. C. Slater and J. G. Kirkwood, Phys. Rev. **37**, 682 (1931).
[25] D. M. Bishop and B. Lam, Chem. Phys. Lett. **143**, 515 (1988).
[26] S. Nir, J. Chem. Phys. **59**, 3341 (1973).
[27] A. V. Gubskaya and P. G. Kusalik, J. Chem. Phys. **117**, 5290 (2002).
[28] L.-Y. Tang, Z.-C. Yan, T.-Y. Shi, and J. F. Babb, Phys. Rev. A **90**, 012524 (2014).
[29] J. Tiihonen, I. Kylänpää, and T. T. Rantala, Phys. Rev. A **91**, 062503 (2015).
[30] B. Champagne, E. Botek, M. Nakano, T. Nitta, and K. Yamaguchi, J. Chem. Phys. **122**, 114315 (2005).
[31] A. D. Buckingham, in *Permanent and Induced Molecular Moments and Long-Range Intermolecular Forces* (John Wiley & Sons, Inc., New York, 2007), pp. 107–142.
[32] H. F. Trotter, Proc. Am. Math. Soc. **10**, 545 (1959).
[33] R. G. Storer, J. Math. Phys. **9**, 964 (1968).
[34] C. Chakravarty, M. C. Gordillo, and D. M. Ceperley, J. Chem. Phys. **109**, 2123 (1998).
[35] D. M. Ceperley, Rev. Mod. Phys **67**, 279 (1995).
[36] I. Waller, Z. Phys. **38**, 635 (1926).
[37] G. L. Sewell, Math. Proc. Cambr. Philos. Soc. **45**, 631 (1949).
[38] C. D. Lin, Phys. Rep. **257**, 1 (1995).
[39] H. Nakashima and H. Nakatsuji, J. Chem. Phys **127**, 224104 (2007).
[40] S. Kar and Y. K. Ho, Phys. Lett. A **372**, 4253 (2008).
[41] J. Pipin and D. M. Bishop, J. Phys. B: At., Mol. Opt. Phys. **25**, 17 (1992).
[42] A. M. Frolov and V. H. Smith, Phys. Rev. A **56**, 2417 (1997).
[43] Z.-C. Yan, J. Phys. B: At., Mol. Opt. Phys. **35**, L345 (2002).
[44] C. L. Pekeris, Phys. Rev. **112**, 1649 (1958).
[45] W. Cencek, K. Szalewicz, and B. Jeziorski, Phys. Rev. Lett. **86**, 5675 (2001).
[46] W. R. Johnson and K. T. Cheng, Phys. Rev. A **53**, 1375 (1996).
[47] M. N. Grasso, K. T. Chung, and R. P. Hurst, Phys. Rev. **167**, 1 (1968).
[48] I. Kylänpää and T. T. Rantala, J. Chem. Phys. **135**, 104310 (2011).
[49] A. V. Turbiner and H. Olivares-Pilon, J. Phys. B: At., Mol. Opt. Phys. **44**, 101002 (2011).
[50] L. Laaksonen, P. Pyykkö, and D. Sundholm, Int. J. Quantum Chem. **23**, 309 (1983).
[51] M. M. Madsen and J. M. Peek, At. Data Nucl. Data Tables **2**, IN3 (1970).
[52] T. Tsogbayar and M. Horbatsch, J. Phys. B: At., Mol. Opt. Phys. **46**, 085004 (2013).
[53] D. M. Bishop and B. Lam, Mol. Phys. **65**, 679 (1988).
[54] W. Kolos and L. Wolniewicz, J. Chem. Phys. **49**, 404 (1968).
[55] D. M. Bishop, J. Pipin, and S. M. Cybulski, Phys. Rev. A **43**, 4845 (1991).
[56] A. V. Turbiner and J. C. Lopez Vieyra, J. Phys. Chem. A **117**, 10119 (2013).
[57] K. Kawaoka, J. Chem. Phys. **55**, 4637 (1971).
[58] K. Pachucki, Phys. Rev. A **85**, 042511 (2012).
[59] M. Pavanello, S. Bubin, M. Molski, and L. Adamowicz, J. Chem. Phys. **123**, 104306 (2005).

[60] S. L. Saito, Nucl. Instrum. Methods Phys. Res., Sect. B **171**, 60 (2000).
[61] M. Stanke, D. Kçedziera, S. Bubin, M. Molski, and L. Adamowicz, J. Chem. Phys. **128**, 114313 (2008).
[62] I. Kylänpää and T. T. Rantala, J. Chem. Phys. **133**, 044312 (2010).
[63] M. Pavanello and L. Adamowicz, J. Chem. Phys. **130**, 034104 (2009).
[64] W.-C. Tung, M. Pavanello, and L. Adamowicz, J. Chem. Phys. **137**, 164305 (2012).
[65] W. Kolos and L. Wolniewicz, J. Chem. Phys. **46**, 1426 (1967).